Investigation on self-noise generation along a simplified towed array sonar

Florian Wachter, Eman Bagheri, Stefan Becker

Institute of Process Machinery and Systems Engineering, 91058 Erlangen, Germany, Email: wa@ipat.uni-erlangen.de

Introduction

Towed array (TA) sonar systems or streamers are horizontally towed underwater sound receivers. In a simplified view, they are designed as long thin elastic tubular cylinders with hydrophones embedded in a viscous fluid in its centre line (Fig. 1).

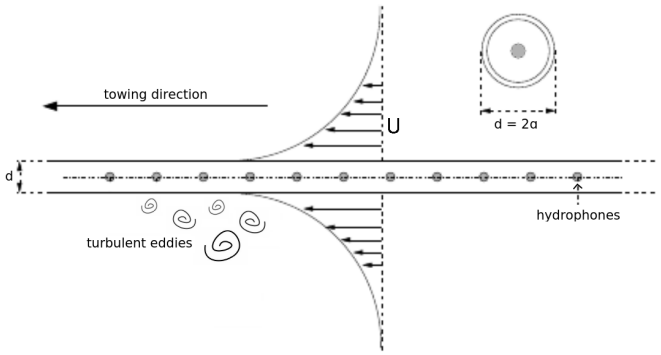

Figure 1: Sketch of a TA that indicates the position of hydrophones, towing direction, relative velocity field U with turbulent boundary layer, diameter d of elastic tube and the corresponding radius a. Modified from [1].

Typically, TA have a large ratio of length to radius a in the order of 10^2 to 10^6 [1]. Due to this ratio and the curvature of the array transversal to the flow, an axisymmetrical turbulent boundary layer (ATBL) develops around the tubular device that has a turbulent boundary layer thickness δ larger than the tube's radius ($\delta/a > 1$). This is demonstrated by a photography from a tow experiment where the ATBL is visualized via dye (Fig. 2).

Figure 2: Visualized ATBL, where the turbulent boundary layer thickness exceeds the radius of the streamer [2].

Axial flow over long circular cylinders are commonly used to study the ATBL around TA. If in such a flow the condition $\delta/a > 1$ is met, curvature effects become significant and lead to changes in the turbulent boundary layer (TBL) compared to the planar case (flat plate or channel flow) and wall-bounded flows along surfaces with only small to moderate curvature transversal to the free-stream direction [3].

Regarding TA, this is interesting because these devices are often limited by flow induced noise that is originated from the turbulent fluctuations within the ATBL. That phenomenon, also known as self-noise, has a negative impact on the signal-to-noise ratio of sonar arrays. The current work aims to investigate the mechanism of self-noise generation and is intended to identify the main excitation sources. Because the literature does not agree on the dominant contributory factor, possible candidates such as the turbulent wall pressure, the fluctuating wall shear stress and the aero- or rather hydro-acoustic source terms are examined, separately. Furthermore, the interaction between the turbulent flow, the deformation of the elastic tube jacket and the interior acoustic of the TA should be analysed through a one-way coupled fluid-structure-acoustic interaction (FSAI) simulation.

Method and Setup

Given the discrepancy in the characteristic scales between flow and sound field, a so-called *hybrid approach* is used by separating the computations of both problems [4]. A basic assumption behind this approach is that the structural deformation and the acoustics are not influencing the flow field (no feedback). The overall procedure is the following. In a first step, the transient flow around a cylinder in axial flow is simulated via finite volume method and a Large Eddy Simulation (LES) with k-equation subgrid model and Van Driest wall damping functions. As simulation platform the open-source code OpenFOAM is used. The radius based Reynolds number $Re_a = aU_\infty/\nu$ is about 10^4, where U_∞ is the freestream velocity and ν the kinematic viscosity. The resulting turbulent wall pressure and wall shear stress fluctuations, as well as the hydro-acoustic source terms, are used in a second step, separately, as input quantities for the mechanic-acoustic simulations. This procedure resembles a one-way coupling between flow and mechanic-acoustic computation and a two-way coupling between the solid mechanics and the acoustics. The latter computation is realized with a finite element method using the scientific code CFS^{++}.

The simulated flow domain and the used numerical grid, that has about 12 million cells, are presented in Fig. 3. The radius of the far-field boundary (f) is 30 times the radius of the cylinder (c) that resembles the TA. The domain length is 10 times the cylinder radius. Periodic boundary conditions are applied in the streamwise direction to realize the axial flow over a long TA.

Fig. 4 is presenting the numerical grid of the mechanic-acoustic simulation. The figure shows the solid mechanic region that represents the elastic tube of the TA (grey),

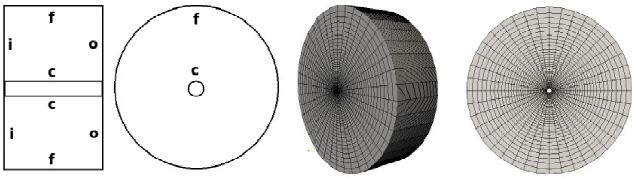

Figure 3: The flow simulation domain sketch in sectional and front view indicates locations of inlet i, outlet o, cylinder wall c and far-field boundary f. The grid resolution in the sketch of the numerical grid is reduced for lucidity.

the interior acoustic region (red) and the outer acoustic region (green). The black squares indicate the boundaries of the acoustic regions where absorbing boundary conditions (ABC) [4] are applied. The black arrow points to the boundary of the solid mechanic region where displacement boundary conditions (DBC) are used. A variety of DBC are tested with major effects on precursory modal analyses but minor effects on the actual mechanic-acoustic simulation. Representatively, this report presents only the results in which the applied DBC suppresses the displacement of both solid boundaries at the end of the tubular cylinder.

The following material parameters are defined for the mechanic-acoustic computation. A thermoplastic polyurethan with a density of $1.12 \cdot 10^3\ kg/m^3$, a Young's modulus of $18.7 \cdot 10^6\ Pa$ and a Poisson number of 0.48 was chosen for the elastic tube of the TA. The defined medium for both acoustic domains is water with a density of $0.997 \cdot 10^3\ kg/m^3$ and a compression modulus of $2.08 \cdot 10^9\ Pa$. Five hydrophones (A-E) are distributed along the centre line of the interior acoustic domain.

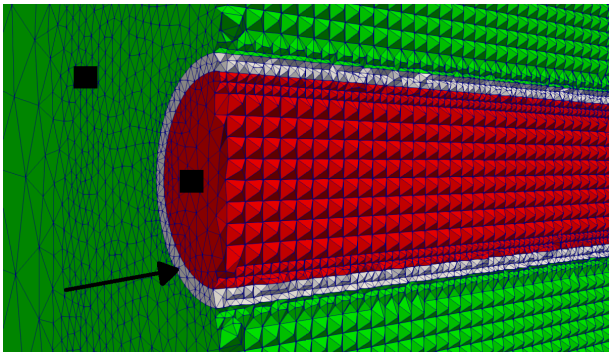

Figure 4: Sectional view on the numerical grid of the mechanic-acoustic simulation showing the solid mechanic region (grey) and the acoustic regions (red, green).

The structural dynamics are defined by Navier's equation while the acoustic wave propagation is described by the linear acoustic wave equation. To investigate the hydro-acoustic source terms the perturbed convective wave equation (*pcwe*) is utilized. The *pcwe* formulation is preferred to other acoustic analogies like Lighthill's inhomogeneous wave equation because it is known to deliver an acoustic field that is free from dynamic flow disturbances [4]. The mechanic-acoustic coupling is realized with the condition that the wall-normal velocity of the mechanical surface is equal to the wall-normal component of the acoustic particle velocity. The simulations should investigate phenomena in a frequency range between 10 and 2000 Hz. The resolution of the numerical grids for the flow and the mechanic-acoustic simulations are well suited for this requirement.

Flow Simulation Results

ATBL are like planar boundary layers two dimensional (in streamwise and wall normal direction) but are subjected to an additional length scale, namely, the radius of the transverse curvature a [3]. Comparable flow conditions in the ATBL exist when the non-dimensional parameters like Re_a, δ/a and the radius in wall units $a^+ = au_\tau/\nu$ are similar. The resulting parameters for the present flow simulations are $Re_a \approx 12300$, $\delta/a \approx 3.6$ and $a^+ \approx 540$. The resulting u_τ (friction velocity) based Reynolds number $Re_\tau = u_\tau\delta/\nu$, that is often used for planar TBL characterization, is about 1900.

Within this section, only some selected results can be presented to show that the physics are captured correctly. In Fig. 5 the so called anisotropy invariant map (AIM) is shown. The AIM uses the trajectory of the invariants $II_a = a_{ij}a_{ji}$ and $III_a = a_{ij}a_{jk}a_{ki}$ which are based on the anisotropy tensor $a_{ij} = \overline{u_iu_j}/q^2 - 1/3\delta_{ij}$, where q^2 is the trace of the Reynolds stress tensor $\overline{u_iu_j}$ and δ_{ij} is the Kronecker delta. The simulation results show AIM trajectories typical for fully developed turbulence of wall-bounded flows [5]. Because the anisotropy tensor is based on the turbulent velocity fluctuations the AIM is a proper tool to verify that the turbulence is captured correctly.

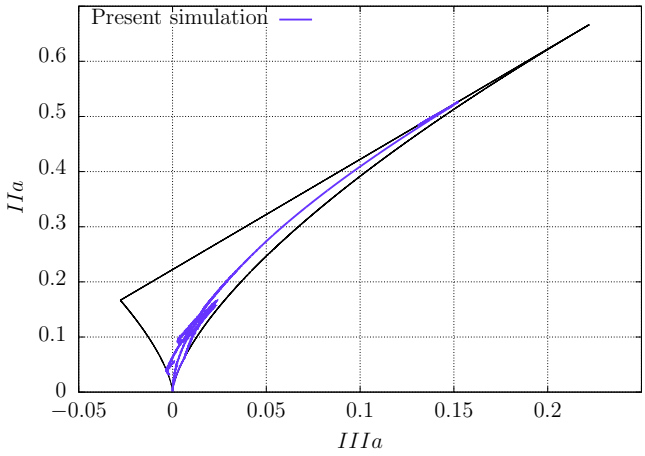

Figure 5: Anisotropy invariant map.

The resulting skin friction coefficient $C_f = 2\tau_w/U_\infty$ that represents the dimensionless wall shear stress τ_w is about 0.0033 and fits well to the literature data and theory stated in [6]. In Fig. 6, the profiles of the root mean square (RMS) pressure fluctuations over the dimensionless wall distance y^+ show a similar behaviour as the included reference data. The values near the wall lie between all shown profiles from literature. However, the maximum values from the simulation are farther away from the cylinder wall. The comparison with included

validation data must be seen sceptically because the dimensionless similarity parameters Re_a, δ/a, a^+, Re_τ are not the same [7] as for the present simulation and also data from channel flow [8] is taken into account. In general, there is only limited ATBL validation data with a comparable set of similarity parameters available in literature [6]. Nevertheless, the included reference data supports that the RMS pressure fluctuations of the present simulation are meaningful.

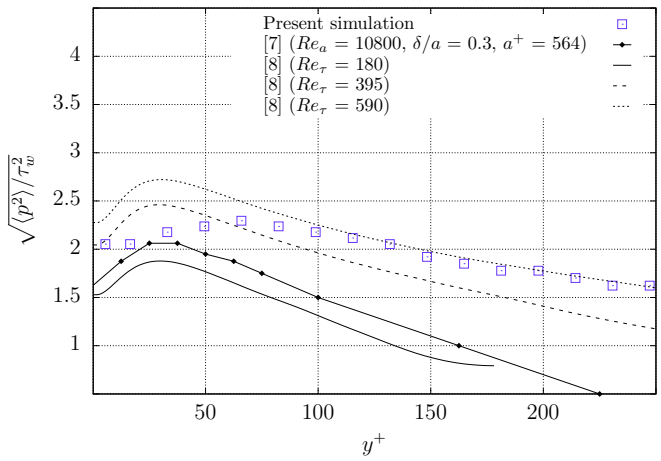

Figure 6: Normalized profiles of the root mean square pressure fluctuations over dimensionless wall distance.

The temporal wall pressure spectrum (Fig. 7) shows the expected trajectory and follows the typical slopes as a function of the angular frequency ω (e.g. ω^{-1}). The simulated data is similar to the spectra of other included wall bounded flows but has more energy contained in the higher frequencies. Once more, due to the limited available literature data and non-matching similarity parameters, the comparison with the references must be carried out carefully. All other results of the flow computation, which can not be shown within this report, also support the aspect of a reliable simulation.

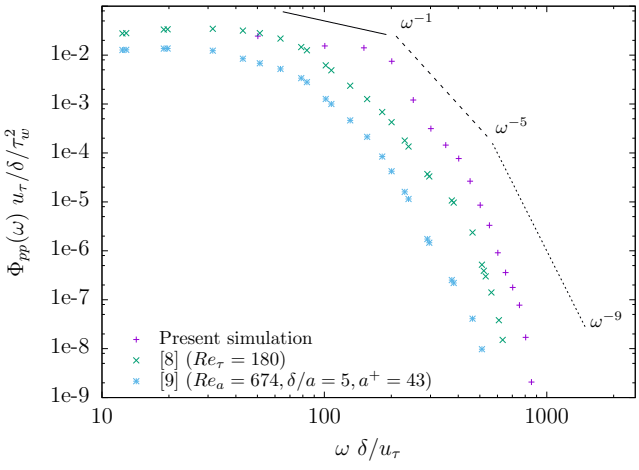

Figure 7: Normalized power spectral density of the instantaneous wall pressure with typical slopes.

Mechanic-Acoustic Simulation Results

Within this section the results of the mechanic-acoustic simulations are presented. As already mentioned in previous chapters the resulting turbulent wall pressure p_w and wall shear stress τ_w fluctuations from the flow simulations are used as an input quantities for the mechanic-acoustic simulation. Additionally, the *pcwe* sources that are located within the ATBL around the tubular cylinder of the TA are utilized as input quantity. The mechanic-acoustic results are presented in Fig. 8. The figure shows the resulting sound pressure level (SPL) of the power spectral density (PSD) of the acoustic pressure that was recorded by the hydrophones. The PSD of all hydrophones are averaged to get one SPL signal related to each single excitation source (p_w, τ_w, *pcwe*). The diagram clearly exhibits that p_w is the dominant source of the induced self-noise in comparison to the other two investigated quantities. The common peaks - for example at 66 Hz - are particularly noteworthy. Due to the fact that p_w is the dominant source further examination is necessary concerning the simulation results from the p_w excitation case.

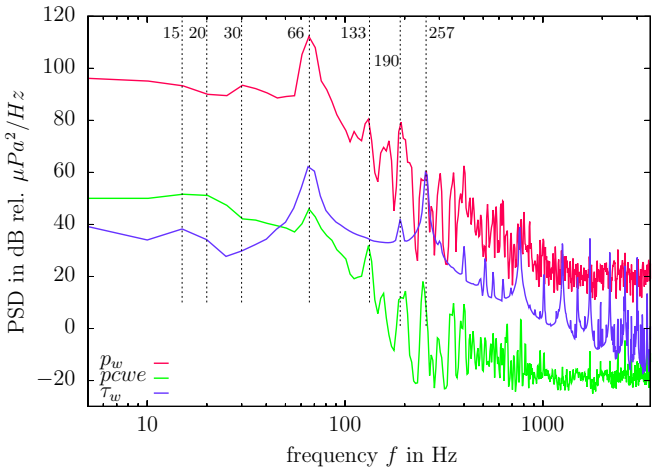

Figure 8: Sound pressure level of the averaged power spectral densities of the acoustic pressure recorded from all hydrophones. Frequencies of certain dominant peaks are indicated.

Fig. 9 is presenting only the results from the mechanic-acoustic simulation with p_w excitation and showing the PSD from all single hydrophones. The spectra reveal a f^{-1} decay for frequencies f up to 100 Hz and a $f^{-5/3}$ decay for higher frequencies. The f^{-1} slope is also visible in the wall pressure spectra (Fig. 7) and coincides with statements from [10] reporting a universal power law decay with the identified slope. The $f^{-5/3}$ slope is typical for turbulent flows and is well known from the energy spectrum of turbulence in the inertial sub-range. Acoustic resonances can not be clearly identified in the spectra. Radial modes are not expect to exist below 44 kHz with the given inner diameter of the tubular cylinder. Axial resonance modes are indeterminable because the acoustic region within the cylinder can be seen as unlimited in axial direction due to the absorbing boundary conditions. However, the dominant peaks (e.g. at 30, 66, 133,

198 Hz) originate from different modes of the tubular structure deformation. This could be identified by using the dynamic mode decomposition (DMD) method. The DMD is able to extract dynamical features from structural deformation associated with a constant oscillating frequency. An example is presented in Fig. 10 for the peak around 66 Hz. The figure shows the max. deformations of the tubular cylinder that could be revealed for 65 Hz via DMD method. It illustrates the superimposition of a bending mode and an alternating breathing mode at the end of the cylinder, both with 65 Hz. These breathing modes explain also the discrepancy of the peak height for the different hydrophones at 66 Hz in Fig. 9. The SPL from hydrophones that are located near the cylinder ends (A,E) are higher, because the more pronounced deformation there leads to locally higher acoustic pressure amplitude. The hydrophone signals located closer to the centre (C,D) show on the contrary lower SPL. The peaks at 30 and 198 Hz also originate from superimposition of two or more structural modes. The peak at 133 Hz originates from a single but more complex radial mode of the structure. Overall, maximum deformations of the tubular structure around 4 μm could be determined by the mechanic-acoustic simulation. This corresponds to a y^+ value of 0.25, which is much smaller than the viscous sub-layer of wall-bounded flows, which justifies the one-way coupling approach of the FSAI.

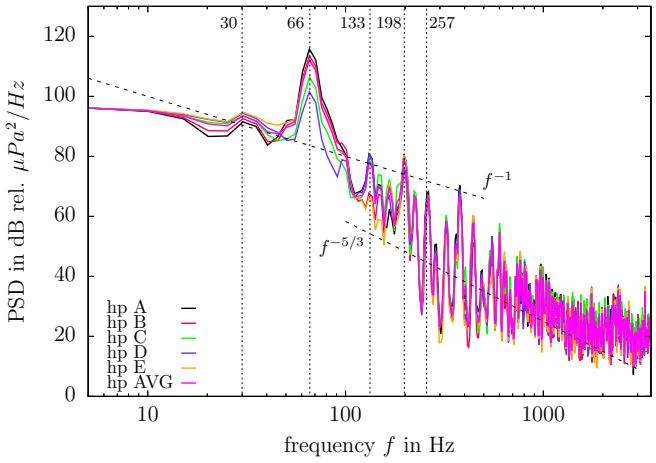

Figure 9: Sound pressure level of the power spectral densities of the acoustic pressure from all hydrophones and from the averaged signal (simulation case with p_w excitation).

Summary and Conclusion

Additional available literature data regarding turbulent statistics of ATBL are desirable for validating the flow simulations. Nevertheless, the AIM and the comparison of results with reference data from other wall-bounded flows show that the simulation gives physically correct results. The mechanic-acoustic computations identify the turbulent wall pressure fluctuation p_w as dominant source for the flow induced self-noise. The resulting spectra from the hydrophone signals show decay slopes that can be related to turbulence. The DMD reveals that the dominant peaks originate from superimposition of different structural deformation modes of the tubular cylinder. The overall maximum deformations of the tubular structure are much lower than the thickness of the viscous sublayer of wall bounded flows what justifies the one-way coupling approach of the FSAI simulation. It must be emphasized that the frequencies associated with the particular structural modes would vary for real TA applications due to the reduced domain length in this work. Nevertheless, the current work was able to answer crucial questions concerning the physics and underlying mechanisms of the self-noise problem.

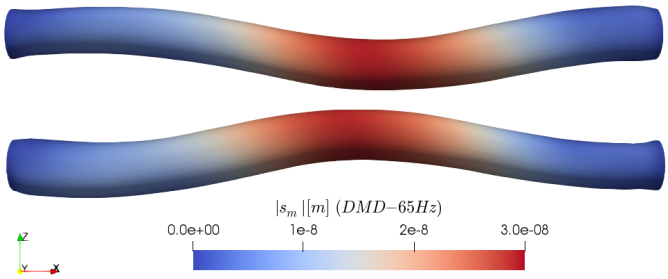

Figure 10: Extracted dynamical features from structural deformation s_m at 65 Hz from DMD method. The two alternating max. deformations are illustrated revealing a superimposition of bending and breathing mode.

References

[1] Abshagen J., Möser M. (Ed.), *Wasserschallmessungen*. Springer Vieweg, Berlin, Heidelberg, 2018.

[2] Elboth T., Wasberg C.E., Helgeland A., Andreassen Ø., Reif B.A.P., *Flow noise simulations around a cylinder*. MekIT'09 5th conference on Computational Mechanics. Tapir Academic Press, 2009.

[3] Lueptow R.M., *Turbulent boundary layer on a cylinder in axial flow*. AIAA journal, 28(10), 1990.

[4] Kaltenbacher M., *Numerical simulation of mechatronic sensors and actuators*. Vol. 3, Springer Verlag Berlin-Heidelberg, 2015.

[5] Jovanovic, J., *The statistical dynamics of turbulence*. Springer Science & Business Media, 2004.

[6] Jordan, S.A., *Near-wall turbulent characteristics along very long thin circular cylinders*. Journal of Fluids and Structures, 27(3), 329-341, 2011.

[7] Woods M.J., *Computation of axial and near-axial flow over a long circular cylinder*. PhD thesis, Mech. Eng. School, University Adelaide, Australia, 2006.

[8] Moser, R.D., Kim, J., Mansour, N.N., *Direct numerical simulation of turbulent channel flow up to Re_τ=590*. Phys. Fluids, vol. 11, pg. 943-945, 1998.

[9] Neves, J.C., Moin, P., Moser, R.D. *Numerical study of axial turbulent flow over long cylinders*. Dep. Mech. Engineering, Stanford University, 1992.

[10] Camussi R., *Noise sources in turbulent shear flows: Fundamentals and applications*. Springer, 2013.